DOI: 10.1111/cgf.12369
Eurographics Conference on Visualization (EuroVis) 2014
H. Carr, P. Rheingans, and H. Schumann
(Guest Editors)

Volume 33 (2014), Number 3

Comparative Blood Flow Visualization for Cerebral Aneurysm Treatment Assessment

R. van Pelt[1], R. Gasteiger[2], K. Lawonn[2], M. Meuschke[2], and B. Preim[2]

[1]Biomedical Engineering, Eindhoven University of Technology, The Netherlands
[2]Visualization Group, Otto-von-Guericke University Magdeburg, Germany

Abstract

A pathological vessel dilation in the brain, termed cerebral aneurysm, bears a high risk of rupture, and is associated with a high mortality. In recent years, incidental findings of unruptured aneurysms have become more frequent, mainly due to advances in medical imaging. The pathological condition is often treated with a stent that diverts the blood flow from the aneurysm sac back to the original vessel. Prior to treatment, neuroradiologists need to decide on the optimal stent configuration and judge the long-term rupture risk, for which blood flow information is essential. Modern patient-specific simulations can model the hemodynamics for various stent configurations, providing important indicators to support the decision-making process. However, the necessary visual analysis of these data becomes tedious and time-consuming, because of the abundance of information. We introduce a comprehensive comparative visualization that integrates morphology with blood flow indicators to facilitate treatment assessment. To deal with the visual complexity, we propose a details-on-demand approach, combining established medical visualization techniques with innovative glyphs inspired by information visualization concepts. In an evaluation we have obtained informal feedback from domain experts, gauging the value of our visualization.

Categories and Subject Descriptors (according to ACM CCS): I.3.8 [Computer Graphics]: Applications—Cerebral Blood Flow I.6.8 [Simulation and Modeling]: Types of Simulation—Combined

1. Introduction

Blood flow information is increasingly consulted for diagnosis and treatment assessment of cardiovascular disease [MFK*12] – currently the leading cause of death worldwide. This work focuses on cerebrovascular conditions, which can cause stroke through blockage or hemorrhage, accounting for approximately one out of nineteen deaths in the USA [GMRea13]. Specifically, we are concerned with cerebral aneurysms, which bear a high risk of rupture, and are therefore related to high morbidity and mortality [SPC09].

An increased number of patient examinations and advances in medical imaging have led to more incidental findings of the mostly asymptomatic cerebral aneurysms [Wie03]. Today, these lesions are often treated with flow diverting stents combined with a coil, promoting thrombosis in the cavity. Initial clinical trials showed promising results, but recent findings show an increased risk of post-treatment hemorrhaging due to a pressure increase [CMR*11].

Neuroradiologists have to assess the treatment risk, depending on the type of stent and its placement; bearing in mind the long-term safety. This process mainly relies on morphological indicators, such as aneurysm size or sphericity. However, this is not reliable in all cases, and the hemodynamics are also evidently important. Current research thus acquires indicators such as pressure and wall-shear stress (WSS) using blood flow simulations [JRST13]. These computational fluid dynamics (CFD) simulations rely on the patient-specific aneurysm morphology, and enable prognostic comparison between different stent configurations.

Besides the quantitative assessment of the simulation outcome, visual analysis is essential to understand the spatial relations between the hemodynamics and morphology [GLvP*12], and is of importance for simulation researchers, stent design engineers and neuroradiologists. The simulations, however, provide an abundance of time-varying hemodynamic information, which should be compared between the stent configurations. To support the visual analysis, a comprehensive visualization is therefore essential.

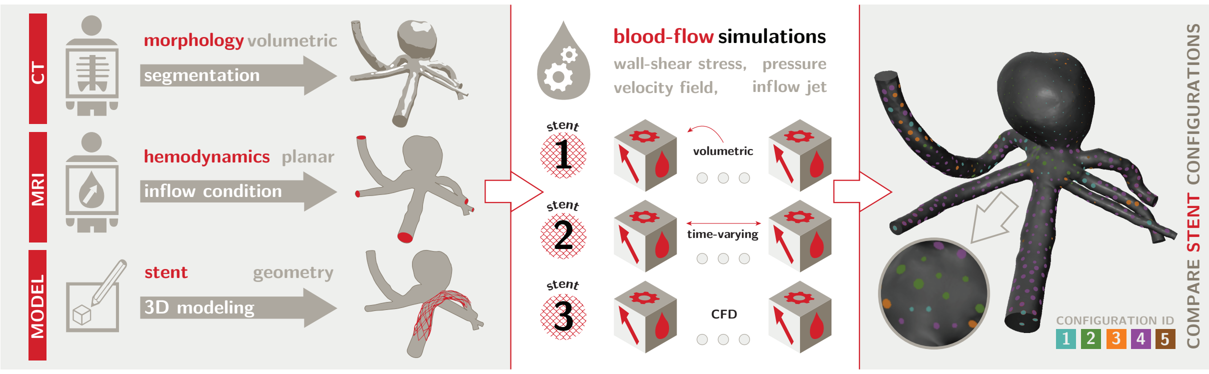

Figure 1: *An overview of the data analysis pipeline. On the left-hand side, the simulation inputs are depicted. Patient-specific morphology is obtained by segmentation of computed tomography (CT) imaging data. Together with this geometry, inflow conditions and different stent configurations are used to model the blood flow behavior. The blood flow simulations, shown in the middle, provide for each stent configuration a time-varying volumetric velocity field, as well as vessel wall characteristics. Visual analysis of this abundance of information is tedious and time-consuming. Therefore, we present a comprehensive comparative visualization that supports the decision-making process for stent placement, as depicted on the right-hand side.*

In this work, we present a comparative visualization for various stent configurations, integrating the aneurysm morphology with simulated blood flow characteristics, e.g., the WSS and aneurysmal inflow. To deal with the visual clutter that arises when directly presenting all these characteristics, we combine established medical visualization techniques with innovative glyphs, based on concepts from information visualization research. Furthermore, we introduce an intuitive details-on-demand approach, facilitating the impact analysis of the different stent configurations.

The main contributions of this work are:

- A comprehensive visualization approach to support the decision-making process for stent placement by facilitating the analysis of various blood flow characteristics in context of the aneurysm morphology. We present an intuitive details-on-demand approach, based on an aggregation of medical visualization techniques with concepts from information visualization.
- An initial evaluation with four domain experts. The informal feedback underpins the value of the visualization.

2. Related Work

An aneurysm bears the risk of rupture at an annual rate of 1% to 2%, causing mortality in 40% to 50% of the ruptured cases [BSH*10]. Morphology provides indicators to assess the rupture risk [SAV*13], which turns out unreliable in several cases. For instance, the rupture risk generally increases with aneurysm size, while rupture of small aneurysms is frequently reported [FBV*01]. Hemodynamics provides unharnessed information for risk and treatment assessment [SPC09]. In current research, simulations are therefore increasingly used prior to intervention, enabling assessment of the blood flow for various treatment options [KTTM08]. Recently, this includes virtual stent deployment to assess different configurations [JRST13].

Besides vessel wall characteristics, the simulations provide time-varying volumetric velocity data. The complex shape and dynamics of the blood flow patterns require visual analysis, but direct representations lead to visual clutter. Recent visualization research has investigated an effective exploration of the intricate blood flow data, incorporating domain knowledge. For instance, line predicates enable selective pathline bundles, such as in regions of high vorticity [BPM*12, KGP*13]. Specifically for cerebral aneurysms, an inflow jet was extracted, depicting the main inflow that affects the surface wall at the so-called impingement zone [GLvP*12]. Despite these advances, several blood flow visualization challenges remain [PB13, vPV13].

The comparison between different stent configurations further complicates the visual analysis, because physician must rely on their memory to judge the differences. To this end, a comparative visualization can facilitate the analysis. Gleicher et al. [GAW*11] proposed a taxonomy that divides comparative designs into three categories: juxtaposition, superposition, and explicit spatial encoding. Juxtaposition shows objects separately, such as the blood flow visualization by Angelelli et al. [AH11], which is effective if comparison takes place within an eyespan. For the complex aneurysm morphology, however, a superposition, or overlay, of objects is more appealing. Also, explicit encoding of the relations between the encoded variables is viable. Verma and Pang [VP04] have presented a range of comparative designs for flow visualization in general. To the best of our knowledge, a comparative design was not previously proposed for treatment assessment in cerebral aneurysms.

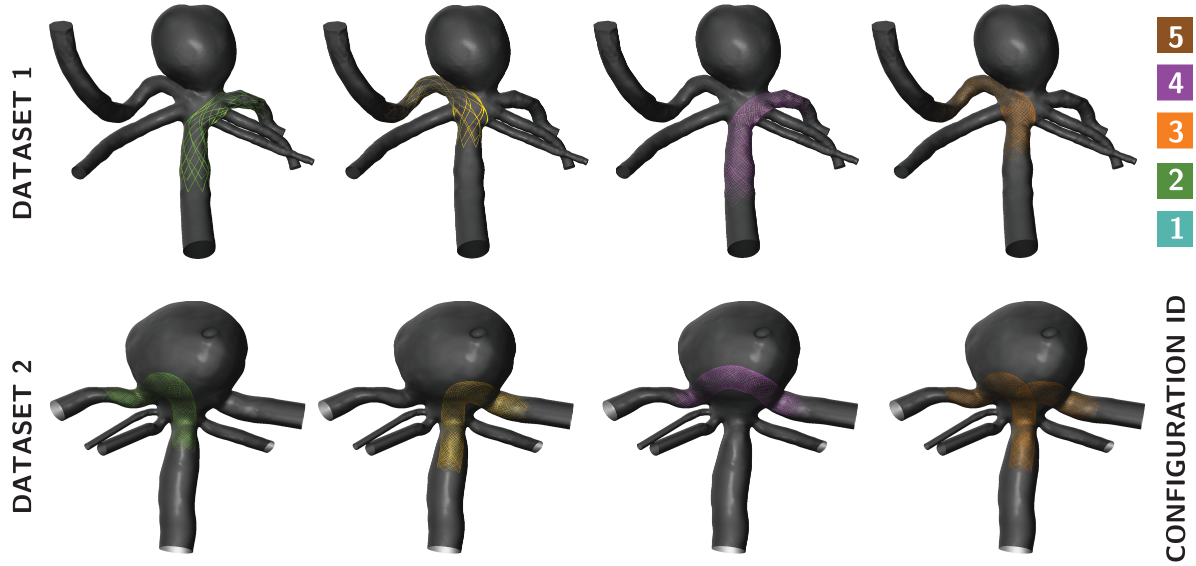

Figure 2: *An overview of the two cerebral aneurysm datasets and their stent configurations. The top row depicts the VISC 2010 data set configurations, comprising from left to right two Neuroform and two SILK type stents, each in different positions. The bottom row depicts a dataset with a known rupture location, visible as a small bulge on the aneurysm sac. For this dataset only the SILK type stent was used. The configuration legend, shown in the top right, consistently encodes the color for the individual configurations of each dataset, where configuration 1 represents the non-stented aneurysm.*

To combine the visualization of the endovascular flow with vessel wall characteristics, sparse representations are required. Therefore, we look at iconic representations, called glyphs, which enable a local interpretation as well as an overall structure given by the glyph arrangement. A taxonomy of glyph visualizations for medical applications was presented by Ropinski et al. [ROP11]. We opt for a composite glyph design, such as presented by Mljenek et al. [MEV*05], taking inspiration from visual encodings and graph designs in the information visualization field [War00].

3. Data Characteristics

As depicted in Figure 1, the CFD simulations rely on patient-specific morphology, obtained through segmentation of anatomical imaging data together with in- and outflow conditions. The overall data is preprocessed according to the pipeline of Gasteiger et al. [GLvP*12]. The boundary conditions are generally defined as two-dimensional planar inlets, either as fixed laminar inflow or MRI acquired blood flow velocity profiles. Besides properties that relate to the interaction between the bloodstream and vessel wall, such as WSS, the simulations also provide volumetric and time-varying velocity fields that describe the endovascular hemodynamics [JRST13].

To assess the treatment options for a specific aneurysm, different types of virtual stents are deployed that tightly fit the patient-specific geometry. The stents consist of a dense strut network of wires, where 8 wires have a diameter of 50 μm and 40 have a diameter of 30 μm. Different brands of stents, e.g., SILK and Neuroform, have a different porosity, leading to different hemodynamics, and hence different treatment outcomes. Moreover, the various types of stents can be positioned differently, as depicted in Figure 2.

To date, clinical research does not agree on the most effective indicators to assess aneurysm development. However, literature describes some potentially relevant vessel wall measures. The rupture risk is larger with an increased wall pressure, mainly caused by systematic hypertension. Moreover, a widely used measure is the WSS – the frictional forces exerted by the bloodstream tangential to the aneurysmal wall. Throughout our work, the term WSS is used to indicate the magnitude of the shear stress vector. Opinions on the relation between WSS and rupture risk are divided into two schools of thought: *low WSS* and *high WSS* [MTXS13]. A *low WSS* is often related to a local stagnation of the blood flow, damaging the intimal layer, and hence weakening the aneurysmal wall which increases the chance of rupture. Alternatively, a *high WSS* leads to remodeling of the vessel wall, leading to an increased rupture risk due to a high mechanical load.

Recent advances in fluid simulations have enabled these extensive patient-specific data, and only few of these datasets are currently available. We have used two datasets of a cerebral aneurysm with different stent configurations, as depicted in Figure 2. The first dataset was provided by the *Virtual Intracranial Stenting Challenge* (VISC) 2010, which became an annual standard test case event in computational minimally-invasive cerebrovascular intervention [RAC*08]. The objective is to challenge academic groups to provide clinical partners with valuable pre-treatment hemodynamic information for a given patient-specific cerebral aneurysm and stent design. For this dataset, two stent types (SILK and Neuroform) were virtually deployed at two different positions. Including the non-stented aneurysm, this results in five configurations, yielding a realistic set of configurations that would be considered in clinical practice. The second dataset was also derived from a clinical dataset, and contains a known rupture location. This location is indicated as small bulge on the backside of the aneurysm sack in Figure 2. For this dataset, only the SILK stent was used and combined to four different positions that also result in five configurations. Based on the stent configuration a different number of volumetric grid points is generated. For the first dataset, the number of velocity data points ranges from 477K – 2,394K with 134K–301K vessel wall data points. The second dataset consists of 775K–1,418K velocity data points and 36K–94K vessel wall data points. In general, the usage of the SILK stent results in a more dense grid due to its lower porosity and smaller wires. Both datasets consist of 20 time steps with a temporal resolution of 50 *ms*.

4. Comparative Visualization

To assess the treatment risk for different stent configurations, we present a comparative blood flow visualization, combining vessel wall information with endovascular blood flow velocity data. The generation of these time-varying data for different configurations is schematically depicted in Figure 1.

The visualization involves two levels of comparison. Primarily, the different stent configurations, depicted in Figure 2, should be compared. Each stent configuration can be visualized using a mouse-over interaction on the configuration legend, rendering the selected stent geometry. The first configuration represents the baseline simulation, without a stent in place. Besides the different configurations, comparison of the temporal hemodynamical variations is required.

Such a comparative visualization for different configurations, incorporating both endovascular and vessel wall information, easily leads to considerable clutter and occlusion. Therefore, we introduce sparse glyph-based representations, combined with an interactive and coherent details-on-demand zooming approach.

4.1. Vessel Wall

An important indicator for the aneurysmal rupture risk is the WSS [SPC09]. Inter-configuration comparison of this continuous vessel wall characteristic requires a sparse representation when combined with the endovascular blood flow information. To this end, we introduce tailored glyph representations that convey the WSS variations between different stent configurations. Throughout the description, we assume the *high WSS* line of thought. Our method also supports emphasis on *low WSS* regions when indicated by the user.

4.1.1. Glyph Distribution

For an effective visualization, proper glyph placement on the vessel surface is crucial. Instead of a data-driven approach, we opt for evenly distributed anchor points on the surface mesh, enabling interactive density adjustment and improving pre-attentive glyph processing. The distribution, inspired by Crane et al. [CWW13], is based on the heat equation:

$$\frac{\partial}{\partial t} u(\mathbf{x},t) = \Delta u(\mathbf{x},t), \tag{1}$$

where $u(\mathbf{x},t)$ describes the heat distribution over time t at the vertex $\mathbf{x}$ and Δ is the Laplacian operator. The Laplacian Δ at a vertex i can be discretized with the cotangent weights:

$$(\Delta u)_i = \frac{1}{2A_i} \sum_{j \in N(i)} (\cot \alpha_{ij} + \cot \beta_{ij})(u_j - u_i), \tag{2}$$

where A_i is one third the area of all incident triangles, $N(i)$ is the neighbor set of i and α_{ij}, β_{ij} are the angles opposing the edge (i, j). We determine the heat distribution by a single implicit Euler step as follows:

$$(I - t \cdot \Delta)u = u_0, \tag{3}$$

where t is a single time step, I is the identity matrix, and u_0 is the initial heat distribution. We start with an initial point i and set $u_0(j) = \delta_{ij}$. For t, we use the same correspondence as in Crane et al. [CWW13], and set $t = mh^2$ with m as a constant and h as the mean of length of all adjacent nodes. With a sparse Cholesky factorization [CDHR08], we are able to solve Eq. 3 for different u_0. First, we solve the heat equation and determine u. Afterwards, we search for the point k with the lowest scalar value, set $u_0(j) = \delta_{ij} + \delta_{kj}$ and solve the heat equation again. This method is repeated until we obtain the desired number of anchor points.

4.1.2. Glyph Representations

We have devised a set of glyphs that exploit both the pre-attentive and the attentive phase in the processing of the visual stimuli [ROP11]. These glyphs enable interactive details-on-demand, using different zoom levels that provide progressively rich information. The coarsest zoom level gives a general overview, anticipating on the pre-attentive processing of the visual system. Zooming in on areas of interest yields a transition to different abstraction levels [vdZLBI11], progressively revealing more information about the different stent configurations and the temporal variations, where attentive analysis enables detailed understanding.

In the following, we describe the glyphs at different zoom levels, depicted in Figure 3, and the level transitions:

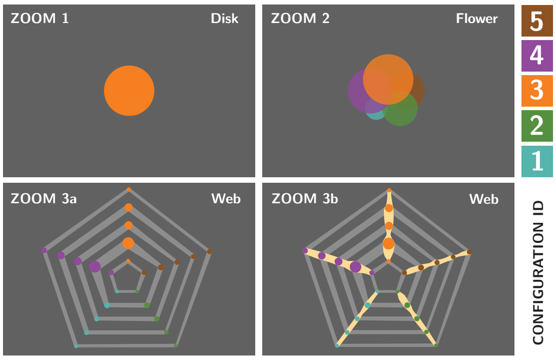

Figure 3: *The proposed glyph set enables details-on-demand using zoom levels. The levels have a coherent transition and provide progressively rich information. The first level shows a disk glyph that conveys the overall maximum WSS. By zooming in, the flower glyphs shows the maximum WSS over time for each stent configuration. The web glyph furthermore conveys the WSS variations in time, first as a subsampling (3a) and finally with time variation strips (3b).*

Zoom level 1: Disk. The first zoom level provides a global overview of the WSS distribution on the vessel wall surface. At each anchor point, a disk glyph represents the largest WSS value for all time phases and all stent configurations. To this end, the diameter of the disk is scaled with the WSS magnitude following Stevens' power law, adjusting for perceptual misjudgement of the WSS value based on the glyph area [WGK10]. For regions with excessive WSS values, the diameter is fixed to the 95 percent quantile of all values. A red outline indicates when this maximum is exceeded.

The different stent distributions are conveyed using contrasting colors, spread in color space. The human visual system can discern only a small number of quantized colors preattentively. This, however, does not pose a limitation, as the number of stent configurations is always sufficiently confined.

Area is not the most suitable visual stimulus for quantitative estimation of the WSS [War00]. However, the scaled disks provide a sparse representation that is suitable for surface visualization. Moreover, the human visual system is susceptible to patterns that emanate from the structure of the overall glyph arrangement, and hence the glyphs preattentively provide a first overview of the WSS information.

Zoom level 2: Flower. Closing in on the vessel surface initiates a transition to the second zoom level. At this level, the maximum WSS for each stent configuration is represented by a separate disk, which is similarly scaled and colored as before. The disks are arranged around the glyph center, based on an outward fanning transition emanating from the disk from zoom level one. Because this arrangement resembles a set of leaves, this glyph is termed *flower*.

The separate disks enable a reliable interpretation of the absolute WSS value per stent configuration, as opposed to representations such as a pie chart or Nightingale plot. For these representations, data values should add up to 100%, and the areas encode a relative value, which is not suitable for our application. Comparison across the vessel surface is facilitated by sorting the disks, showing the configuration with the largest WSS value on top. The disks are furthermore semi-transparent, enabling comparison of the differences between the configurations.

Zoom level 3: Web. Moving in even closer to the vessel surface activates the *web glyphs*. In addition to the WSS for different stent configurations, the glyph at this zoom level also reveals the temporal variations. Therefore, temporal subsamples of the WSS are positioned along evenly distributed axes, resembling the established star plot approach [CCKT83]. Starting from the flower glyph, this arrangement arises intuitively from a fanning out transition. To maintain the anatomical relation, the glyphs are positioned tangential to the vessel surface, and their orientation is fixed in object space to avoid mentally disturbing realignment upon exploration.

At this zoom level, time is discretized into a fixed number of five samples for each stent configuration, depicted by disk glyphs similar to the aforementioned flower disks. The time samples capture the main phases of the cardiac cycle: systole and diastole. The first three time samples convey the WSS in the systolic phase, while the heart muscle contracts. Starting from the central sample, the last two samples convey the diastolic phase, when the heart refills with blood. Note that the second and fourth time sample characterize the WSS respectively at peak systole and peak diastole, which are key time points for blood flow analysis.

As depicted in Figure 3, this zoom level is divided into two sublevels. At zoom level 3*a*, the time sample disks are connected to adjacent axes with a gray ribbon, facilitating inter-configuration comparison. The most detailed web glyph is shown at zoom level 3*b*, which adds a yellow time ribbon along the axes. Besides the subsampled time steps represented by the disks, the ribbon width encodes the fine-grained WSS variations over time.

These zoom levels enable an exploration of the WSS, gradually revealing more information. To facilitate the visual comparison, we have designed the glyph set such that the cognitive load is limited. No animation is used to convey the temporal variations, and juxtaposed comparisons are within an eyespan. The flower glyphs are based on superposition of the disks, but the web glyphs rely on a short distance juxtaposed comparison between the axes, which is further supported by the gray ribbons that connect the time samples.

In zoom level 3, the WSS variations of a configuration can only be compared to the two configurations that are adjacent in the web glyph. With some more effort, visual comparison to other configurations is feasible. The comparison process,

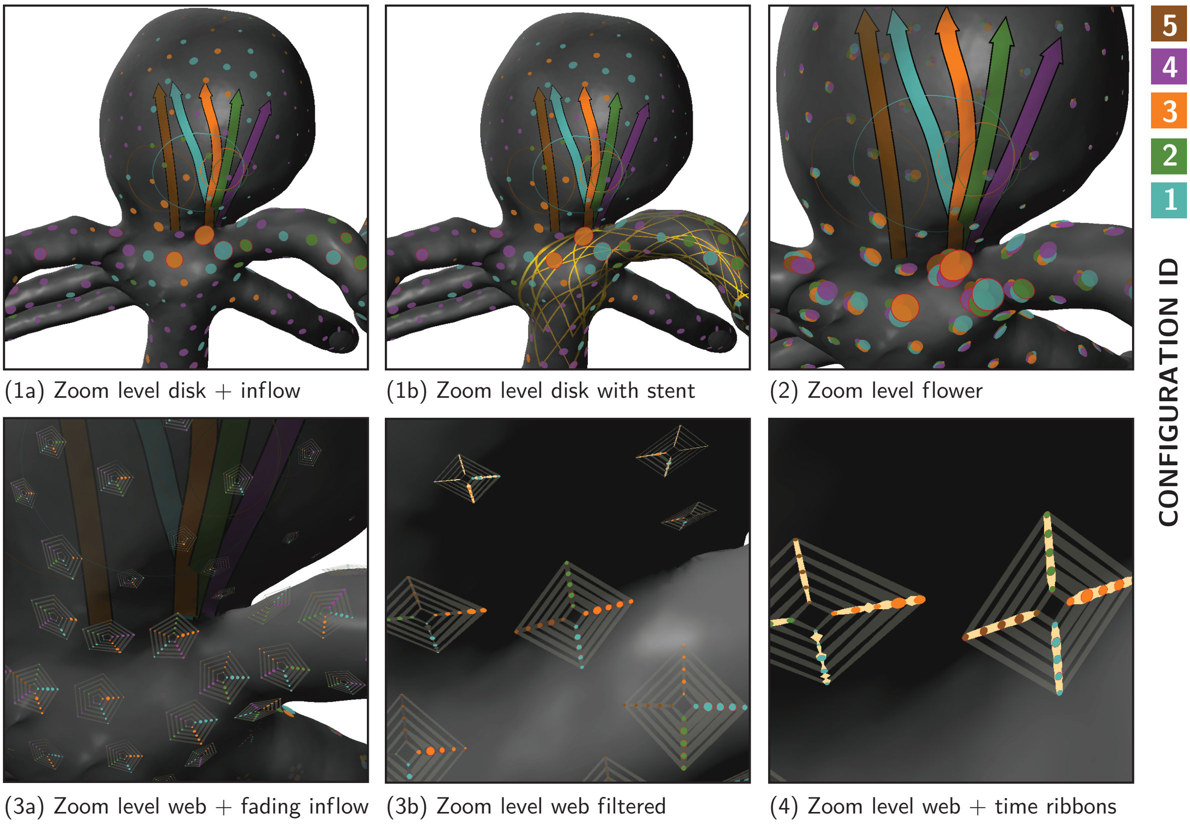

Figure 4: *The proposed workflow for exploration (dataset 1). (1a) Assess the overview using disk glyphs combined with the endovascular flow, depicted by the inflow jets (arrow glyphs) and impingement zones (contours). (1b) Hovering the mouse over the configuration legend shows the stent geometry. (2) Zooming in reveals the flower glyphs, enabling comparison of the maximum WSS between configurations. (3a) Closing in further, the web glyphs show the temporal WSS variation using five subsamples. (3b) Configuration four is omitted. (4) Time ribbons give more details on the temporal WSS variation.*

however, is further supported by an interactive filtering approach. When a stent configuration is discarded, based on the assessment of the WSS values, it can be omitted from the visualization. The glyphs will automatically rearrange, which for the web glyph means that other stent configurations will be displayed alongside each other.

4.2. Endovascular Blood Flow

The sparsity of the glyphs allows to combine the vessel wall visualization with a representation of the endovascular blood flow. Therefore, we employ a domain-specific abstract representation of the time-varying volumetric velocity data. On the one hand, the endovascular blood flow is largely characterized by a high-speed inflow into the aneurysm sac, called the *inflow jet*. On the other hand, the region where the inflow jet has a considerable impact on the vessel wall is of importance. This region is known as the *impingement zone*. A concentrated inflow jet with a narrow impingement zone indicate an increased rupture risk [CMWP11].

We extract the inflow jet and impingement zone for each stent configuration according to the definitions by Gasteiger et al. [GLvP*12]. As shown in Figure 4, the inflow jets are depicted by an abstract arrow glyph; consistently color-coded according to the configuration it represents. Furthermore, the impingement zones are presented as outlines on the vessel wall surface, which are similarly color-coded.

Visibility of the inflow jet arrow glyphs is ensured by transparency of the front faces of the vessel wall surface. To avoid visual clutter at the more detailed zoom levels, i.e., levels 2 and 3, we have incorporated an opacity modulation that depends on the distance to the surface. While zooming in, the front faces of the surface become more opaque, gradually hiding the inflow jet glyphs, while enabling an uncluttered view of the glyphs. Since the inflow jet is mainly of importance in context of the global overview, no relevant information is lost by hiding the arrows when zooming in.

4.3. Workflow

To select the most suitable stent configuration, we propose a workflow that facilitates comparison of the abundance of data for the different stent configurations. The workflow consists of a stepwise exploration, based on the described vessel wall and endovascular blood flow visualization, which converges to the selection of the preferred stent configuration.

The workflow, depicted in Figure 4, starts with a visual assessment at zoom level 1. At this overview level, the disk glyphs give a first impression of the WSS, and hence which stent configuration is eligible to be omitted. This level furthermore depicts the inflow jets and associated impingement zones on the vessel wall. Additionally, the stent geometries can be visualized at any time by hovering over the configuration legend with the mouse.

Based on the distribution of the WSS distribution as well as the domain knowledge of the aneurysm anatomy, the user can subsequently zoom in to level 2. The flower glyphs allow for a more detailed comparison between the stent configuration at the regions of interest. With the *high WSS* point of view, the user would look for the configuration that has a low WSS on the aneurysm sac, while the WSS should be substantially larger than the non-stented configuration in the parent vessel compared. For example, in Figure 4 configuration five shows a comparatively low WSS in the parent vessel, and may be omitted using the filtering technique.

At this point, the user likely has a preferred stent configuration in mind. The final step is used to confirm the initial choice. Therefore, details on the WSS variations over time can be inspected at zoom level 3 at specific regions of interest. The subsampled time variations provide a sufficient summary for most cases, but the most comprehensive details can be inspected at zoom level 3b. We propose this workflow to effectively compare the hemodynamic information of the different stent configurations to support the treatment assessment. This workflow, however, is not fix but enables an exploratory analysis.

4.4. Implementation

We have implemented our approach in the C++ programming language, supported by the Visualization Toolkit (VTK), the OpenGL library, and the GLSL shading language. On a standard mid-class desktop (Intel i7, quad core, 2.3GHz, 16GB RAM, GeForce GTX 660) we achieve interactive frame rates of about 40 FPS for the dataset with the largest number of vessel wall data points. We perform the glyph rendering completely on the GPU by extensively using the geometry shader stage. For this, the position and normal of each anchor point are processed by the vertex shader stage of the GPU via vertex buffer objects (VBOs). An additional VBO is used to store a mipmap ID for each anchor point to provide a flexible filtering of the anchor point density later. Furthermore, we send several textures to the GPU that contain mainly the normalized scalar information at each anchor point for each configuration and time step, the color values for each configuration as well as the configuration IDs that my be filtered out by the user during run time.

In the geometry shader stage, each incoming point primitive is converted into a triangle strip that represents a tangent aligned quad at each anchor point. Additionally, texture coordinates are assigned. Depending on the glyph set and corresponding scalar value, each quad is scaled and shifted to its final position. The connection and time ribbons in the web glyph set are also represented with quads and generated by additional invocations of the corresponding geometry shader. The transition animation between each zoom level is achieved by incorporating the length of the vessel surface bounding box diagonal. If the distance of the camera to each anchor point is between certain length thresholds, the transition and fading between each glyph set are performed. The disk shape is computed procedurally in the fragment shader stage by solving the equation of a circle on the texture coordinates of the quad fragments.

The final composed visualization is accomplished by a full-screen multi-pass rendering with several offscreen rendered images that include the vessel surface, the glyph sets, inflow jets and impingement zones as well as the stent geometries. The front faces of the vessel surface are rendered with the ghosted view approach presented in Gasteiger et al. [GNKP10] to ensure both surface shape information and visibility of the embedded inflow jet representations. The view-aligned inflow jet arrow glyphs are rendered with the method proposed by Gasteiger et al. [GLvP*12].

5. Evaluation

The presented comparative visualization was established in close consultation with domain experts. The results were evaluated with two CFD engineers with expertise in patient-specific blood flow simulations, and two clinicians with expertise in aneurysm treatment and blood flow analysis. The informal evaluation study involved a comparison between the conventional juxtaposed grid and our visualization, as depicted in Figure 5, aiming to understand which method best supports the needed exploration. The juxtaposed views were fully linked, presenting the five stent configurations for five evenly-spaced time steps, with the WSS encoded by a black-body radiation color map.

All participants were asked to explore the data and identify configurations that correspond to certain WSS characteristics, e.g., high WSS at the aneurysm neck. Both CFD engineers stated that the juxtaposed grid is hard to interpret, requiring a repeated change of focus between the views. The clinical experts were more familiar with this kind of presentation due to their clinical usage of side-by-side views of medical image datasets for diagnoses and treatment. Although a comparison along a configuration row or along a

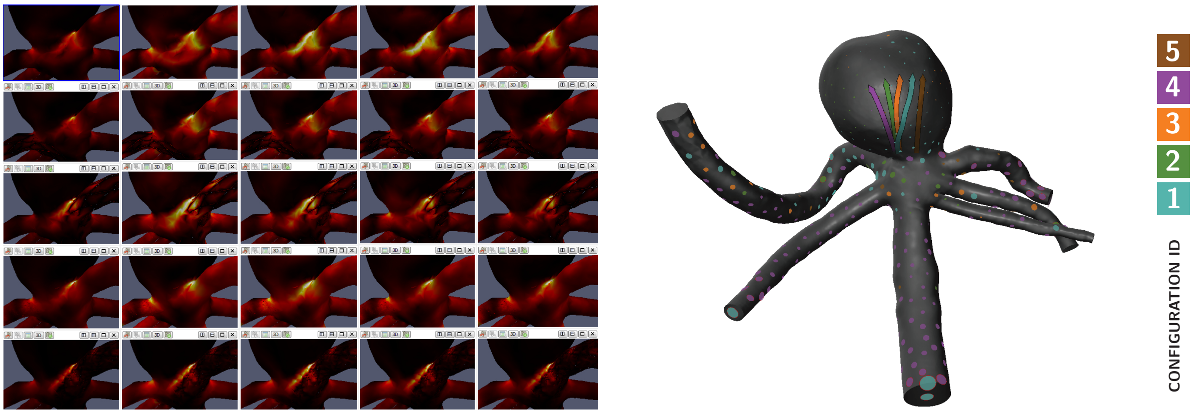

Figure 5: *An informal evaluation was conducted with domain experts. They were presented with the established juxtaposed grid visualization (left) to compare the hemodynamic information of different stent configurations, and were asked to compare this to our comparative visualization approach (right). Besides the WSS values on the vessel wall, our approach furthermore superimposes endovascular blood flow information, e.g., the inflow jets (dataset 1).*

time step column is feasible they stated that it is quite difficult to compare between individual views.

The participants then assessed our comparative visualization and the established juxtaposed grid. They all required a small amount of time to familiarize themselves with the glyphs, but quickly appreciated the integrated view. At the first zoom level, the inflow jets and impingement zones were considered valuable for comparison of the hemodynamic characteristics. The impingement zone size was considered important and some of the participants discarded those configurations leading to a small impingement zone.To assess the impingement zone more reliably, the participants would like to know the speed of the inflow jet. All participants valued the selective stent embedding, mentally connecting the configuration color and stent position. The configuration filtering capability was deemed very useful. One clinician used the filtering to sequentially inspect the configurations. Without the inflow jet and impingement zone visualization, important information would be missing.

The participants focused on various locations on the aneurysm surface, e.g., the neck or the rupture location, investigating the WSS magnitudes between the configurations at the flower zoom level. For more details, the CFD engineers zoomed to the web glyphs level. One CFD engineer stated that this zoom level was supportive for assessment of local WSS variations over time, including variations between the configurations. Regional and dynamic effects were harder to assess, as comparison of neighboring web glyphs requires cognitive effort. The additional time strips of the web glyphs were considered of lesser importance. Only a few relevant time steps are typically considered: the first time step and the peak systolic and diastolic time steps. The clinicians mostly consider only peak systole. Hence, the disk and flower zoom level were considered most relevant.

One participant suggested a visual distinction of the first configuration, which is not stented, from other configurations. The uniform point distribution and its density adjustment was appreciated. However, a user-defined definition of anchor points was requested, e.g., at bulges or within the impingement zone, as well as a surface selection that restricts the region where anchor points are visible. Also, a legend that relates the disk glyph size to quantitative values was requested, facilitating visual approximation of the WSS values. An interaction to obtain quantitative values is desirable.

The evaluation yielded several points for improvement.Since the evaluation, we have for instance incorporated the user-defined anchor point definition and adjusted the legend with textual annotations to clarify the configuration setting as desired by some participants. In summary, the CFD engineers considered our method as an improvement over the juxtaposed grid visualization and the clinical experts valued our approach as a meaningful overview visualization that complements the grid visualization and has potential to support the therapy planning process.

6. Discussion

The main motivation for our comparative visualization is to support neuroradiologists in the decision-making process. The extensive simulation of multiple stent configurations is, however, a highly specialized task, and is still actively investigated by biomedical researchers. Consequently, these data are not yet part of clinical practice, and the presented visualization therefore currently provides a valuable tool for simulation researchers. The comparative visualization can be employed as part of the reporting process, compactly depicting the large amount of hemodynamic information. Furthermore, stent engineers could benefit from our visualization in the process towards personalized stent designs.

Figure 6: *Stent configuration assessment visualization for dataset 2: the ruptured case. Configurations 5 appears most suitable, since it results in a low WSS on the aneurysm and exhibits a large impingement zone.*

As an example, Figure 6 shows the transition from the disk to the flower representation for dataset 2, with a view on the ruptured location. Additionally, the inflow jets and their impingement zones are depicted for each of the configuration. Around the rupture location, stent configuration 2 and 4 result in a high WSS distribution. Following the *high WSS* theory, these two potential treatment configurations appear less suitable. The vessel surface region around the rupture is still likely to be weak, and hence a high WSS increases the risk of a repeated rupture. Looking at the impingement zone, however, configuration 4 seems to be a viable option because of the large impingement area. A large zone typically indicates a diffuse inflow jet, and is associated with a lower risk of rupture. Configuration 3 and 5 consist both of a large impingement zone but configuration 5 is less prominent in terms of the WSS distribution (see Fig. 6). Thus, this configuration represents the most appropriate stent in that particular case, which was also confirmed by the clinicians working with our approach. This underpins that our comparative visualization provides the essential information, enabling a selection of the preferred configuration for which the stent geometry can be embedded. Furthermore, the inflow jet without a stent, in configuration 1, is considerably different, resulting in a small impingement zone and large WSS distribution. This confirms a high rupture risk.

As opposed to a pure quantitative assessment of the simulation results, our visualization shows the abundance of information in the spatial context of the anatomy. With the glyph design, we limit the cognitive load to perform the visual comparison. Direct inter-configuration comparison in the web glyph is, however, restricted to the two neighboring axes. This issue is inherent to visual comparison, and is largely resolved by the presented filtering approach. Alternatively, a sorting approach is conceivable.

In this work, the prevailing WSS measure is employed as the dominant vessel wall characteristic for assessment of the rupture risk. However, the presented glyph set can be used for various surface measures, maintaining the details-on-demand approach. Examples of alternative measures include the wall pressure, the oscillatory shear index, and the relative residence time.

7. Conclusions and Future Work

Contemporary blood flow simulations provide comprehensive hemodynamic information for various stent configurations in a cerebral aneurysm, supporting the assessment of rupture risk prior to treatment. However, visual comparison is complicated, because the abundance of information induces a high cognitive load. In contrast to the prevailing juxtaposed grid view, we have proposed a comparative visualization that combines morphology with widely used blood flow indicators. To deal with the visual complexity, we introduced a glyph set that enables interactive details-on-demand, combined with an abstract representation of the endovascular blood flow.

To assess the effectiveness of our comparative visualization, we have conducted an informal evaluation with domain experts. The participants assessed the hemodynamic information using the established juxtaposed grid visualization, and compared this to our integrated visualization. The respondents appreciated our comparative approach better than conventional juxtaposed grid visualization. With some improvements, including a legend to approximate WSS values and further integration of quantitative information, our visualization would be adopted by the domain experts. The feedback was mainly positive, and hence we believe that the comparative visualization has potential to become part of the clinical treatment planning.

In future work, the informal evaluation provides a basis for a quantitative perceptual user study, which is needed to achieve clinical adoption. In such a study, our approach could be compared with the juxtaposed grid, asking participants to fulfill representative tasks that domain experts need to perform. This might include identification of maximum WSS areas among the configurations, as well as the stent configuration with optimal performance. The two visualization approaches should be evaluated with respect to the participants' accuracy, response time and their personal preferences. Such a study should also assess the influence of the design decisions on the task performance; for instance, the perceptual consequences of the flower glyph scaling or the web glyph orientation for local comparison.

Acknowledgments

The authors would like to thank U. Preim (Hospital Magdeburg, Germany), O. Beuing (University Hospital Magdeburg, Germany), G. Janiga and P. Berg (ISUT, University Magdeburg, Germany) for participating in the evaluation.This work was partly funded by the German BMBF project *STIMULATE* (grant no. 03S016101A).

References

[AH11] ANGELELLI P., HAUSER H.: Straightening tubular flow for side-by-side visualization. *IEEE Transactions on Visualization and Computer Graphics 17*, 12 (2011), 2063–2070. 2

[BPM*12] BORN S., PFEIFLE M., MARKL M., GUTBERLET M., SCHEUERMANN G.: Visual analysis of cardiac 4D MRI blood flow using line predicates. *IEEE Transactions on Visualization and Computer Graphics 19*, 6 (2012), 900–912. 2

[BSH*10] BAHAROGLU M., SCHRIRMER C., HOIT D., GAO B.-L., MALEK A. M.: Aneurysm inflow-angle as a discriminant for rupture in side- wall cerebral aneurysms morphometric and computational fluid dynamic analysis. *Stroke 41*, 7 (2010), 1423–1430. 2

[CCKT83] CHAMBERS J., CLEVELAND W., KLEINER B., TUKEY P.: *Graphical Methods for Data Analysis*. Wadsworth, 1983. 5

[CDHR08] CHEN Y., DAVIS T. A., HAGER W. W., RAJAMANICKAM S.: Algorithm 887: Cholmod, supernodal sparse cholesky factorization and update/downdate. *ACM Transactions on Mathematical Software 35*, 3 (2008), 22:1–22:14. 4

[CMR*11] CEBRAL J. R., MUT F., RASCHI M., SCRIVANO E., CERATTO R., LYLYK P., PUTMAN C. M.: Aneurysm rupture following treatment with flow-diverting stents: computational hemodynamics analysis of treatment. *American Journal of Neuroradiology 32*, 1 (2011), 27–33. 1

[CMWP11] CEBRAL J. R., MUT F., WEIR J., PUTMAN C. M.: Quantitative characterization of the hemodynamic environment in ruptured and unruptured brain aneurysms. *American Journal of Neuroradiology 32*, 1 (2011), 145–151. 6

[CWW13] CRANE K., WEISCHEDEL C., WARDETZKY M.: Geodesics in heat: A new approach to computing distance based on heat flow. *ACM Transactions on Graphics 32*, 5 (2013), 152:1–152:11. 4

[FBV*01] FORGET T. R. J., BENITEZ R., VEZNEDAROGLU E., SHARAN A., MITCHELL W., SILVA M., ROSENWASSER R. H.: A review of size and location of ruptured intracranial aneurysms. *Neurosurgery 49*, 6 (2001), 1322–1326. 2

[GAW*11] GLEICHER M., ALBERS D., WALKER R., JUSUFI I., HANSEN C. D., ROBERTS J. C.: Visual comparison for information visualization. *Information Visualization 10*, 4 (2011), 289–309. 2

[GLvP*12] GASTEIGER R., LEHMANN D. J., VAN PELT R., JANIGA G., BEUING O., VILANOVA A., THEISEL H., PREIM B.: Automatic detection and visualization of qualitative hemodynamic characteristics in cerebral aneurysms. *IEEE Transactions on Visualization and Computer Graphics 18*, 12 (2012), 2178–2187. 1, 2, 3, 6, 7

[GMRea13] GO A. S., MOZAFFARIAN D., ROGER V. L., ET AL.: Heart disease and stroke statistics - 2013 update. *Circulation 127*, 1 (2013), e6–e245. 1

[GNKP10] GASTEIGER R., NEUGEBAUER M., KUBISCH C., PREIM B.: Adapted surface visualization of cerebral aneurysms with embedded blood flow information. In *EG Workshop on Visual Computing for Biology and Medicine* (2010), pp. 25–32. 7

[JRST13] JANIGA G., RÖSSL C., SKALEJ M., THÉVENIN D.: Realistic virtual intracranial stenting and computational fluid dynamics for treatment analysis. *Journal of Biomechanics 46*, 1 (2013), 7–12. 1, 2, 3

[KGP*13] KÖHLER B., GASTEIGER R., PREIM U., THEISEL H., GUTBERLET M., PREIM B.: Semi-Automatic vortex extraction in 4D PC-MRI cardiac blood flow data using line predicates. *IEEE Transactions on Visualization and Computer Graphics 19*, 12 (2013), 2773–2783. 2

[KTTM08] KIM M., TAULBEE D. B., TREMMEL M., MENG H.: Comparison of two stents in modifying cerebral aneurysm hemodynamics. *Annals of Biomedical Engineering 36*, 5 (2008), 726–41. 2

[MEV*05] MLEJNEK M., ERMEST P., VILANOVA A., VAN DER RIJT R., VAN DEN BOSCH H., GERRITSEN F., GRÖLLER M.: Profile flags: a novel metaphor for probing of T2 maps. In *IEEE Visualization* (2005), pp. 599–606. 3

[MFK*12] MARKL M., FRYDRYCHOWICZ A., KOZERKE S., HOPE M., WIEBEN O.: 4D flow MRI. *Journal of Magnetic Resonance Imaging 36*, 5 (2012), 1015–1036. 1

[MTXS13] MENG H., TUTINO V., XIANG J., SIDDIQUI A.: High WSS or low WSS? Complex interactions of hemodynamics with intracranial aneurysm initiation, growth, and rupture: toward a unifying hypothesis. *American Journal of Neuroradiology* (2013). (preprint). 3

[PB13] PREIM B., BOTHA C.: Visual Exploration of Simulated and Measured Flow Data. In *Visual Computing for Medicine*. Morgan Kaufmann Publishers, 2013. 2

[RAC*08] RADAELLI A., AUGSBURGER L., CEBRAL J., OHTA M., RÜFENACHT D., BALOSSINO R., BENNDORF G., HOSE D., MARZO A., METCALFE R., ET AL.: Reproducibility of haemodynamical simulations in a subject-specific stented aneurysm model - a report on the virtual intracranial stenting challenge 2007. *Journal of Biomechanics 41*, 10 (2008), 2069–2081. 4

[ROP11] ROPINSKI T., OELTZE S., PREIM B.: Survey of glyph-based visualization techniques for spatial multivariate medical data. *Computers & Graphics 35*, 2 (2011), 392–401. 3, 4

[SAV*13] SCHNELL S., ANSARI S. A., VAKIL P., WASIELEWSKI M., CARR M. L., HURLEY M. C., BENDOK B. R., BATJER H., CARROLL T. J., CARR J., MARKL M.: Three-dimensional hemodynamics in intracranial aneurysms: influence of size and morphology. *Journal of Magnetic Resonance Imaging 39*, 1 (2013), 120–131. 2

[SPC09] SFORZA D. M., PUTMAN C. M., CEBRAL J. R.: Hemodynamics of cerebral aneurysms. *Annual Review of Fluid Mechanics 41* (2009), 91–107. 1, 2, 4

[vdZLBI11] VAN DER ZWAN M., LUEKS W., BEKKER H., ISENBERG T.: Illustrative molecular visualization with continuous abstraction. *Computer Graphics Forum 30*, 3 (2011), 683–690. 4

[VP04] VERMA V., PANG A.: Comparative flow visualization. *IEEE Transactions on Visualization and Computer Graphics 10*, 6 (2004), 609–24. 2

[vPV13] VAN PELT R., VILANOVA A.: Understanding blood-flow dynamics: challenges in visualization. *IEEE Computer 46*, 12 (2013), 60–67. 2

[War00] WARE C.: *Information Visualization*, vol. 2. Morgan Kaufmann San Francisco, 2000. 3, 5

[WGK10] WARD M., GRINSTEIN G., KEIM D.: *Interactive data visualization: foundations, techniques, and applications*. AK Peters, Ltd., 2010. 5

[Wie03] WIEBERS D.: Unruptured intracranial aneurysms: natural history, clinical outcome, and risks of surgical and endovascular treatment. *The Lancet 362*, 9378 (2003), 103–110. 1